LIMNOLOGY AND OCEANOGRAPHY
Letters

Open Access

Limnology and Oceanography Letters 9, 2024, 716–724

doi: 10.1002/lol2.10404

LETTER

Assessing N_2 fixation flux and its controlling factors in the (sub)tropical western North Pacific through high-resolution observations

Xinran Yu[1,2] *Zuozhu Wen*[1,3] *Ruotong Jiang*[1,2] *Jin-Yu Terence Yang*[1,3] *Zhimian Cao*[1,3] *Haizheng Hong*[1,2] *Yuntao Zhou*[4]* *Dalin Shi*[1,2,3]*

[1]State Key Laboratory of Marine Environmental Science, Xiamen University, Xiamen, China; [2]College of the Environment and Ecology, Xiamen University, Xiamen, China; [3]College of Ocean and Earth Sciences, Xiamen University, Xiamen, China; [4]School of Oceanography, Shanghai Jiao Tong University, Shanghai, China

Scientific Significance Statement

The (sub)tropical western North Pacific has been hypothesized to be a region of intense nitrogen (N_2) fixation. However, the fixation rate, flux, distribution patterns, and environmental controls are poorly understood. To fill this knowledge gap, high-resolution observations and machine learning were conducted. The N_2 fixation rate observed in this region ranged from below the limits of detection to nearly 31 nmol N L^{-1} d^{-1}. Models estimate that this region has a N_2 fixation flux of 5.72 to 6.45 Tg N yr^{-1}. Sea surface temperature, photosynthetically available radiation, and nutrient supply, including iron, phosphate, and nitrogen, were most correlated with the spatiotemporal patterns of N_2 fixation, which were estimated by machine learning. Our findings emphasize the importance of N_2 fixation in this region to global ocean N_2 fixation and its broader implications for marine productivity.

Abstract

The (sub)tropical western North Pacific is potentially an area of intense nitrogen (N_2) fixation in the global ocean, despite limited understanding of the flux and controlling factors. We conducted high-resolution observations from 2016 to 2021 in this region and used machine learning algorithms to simulate N_2 fixation flux. Models estimated an N_2 fixation flux from 5.72 to 6.45 Tg N yr^{-1}, with strong seasonal variation and peak rates in summer. The western North Pacific Subtropical Gyre and the Kuroshio Current contributed more to N_2 fixation flux than did the adjacent areas. Models suggested that sea surface temperature, photosynthetically available radiation, and nutrient supply were most strongly correlated with seasonal and spatial variations in N_2 fixation. This study provides an improved estimation of N_2 fixation in the western North Pacific and advances our understanding of its role in ocean productivity.

*Correspondence: ytzhou@sjtu.edu.cn; dshi@xmu.edu.cn

Associate editor: Angelicque White

Author Contribution Statement: DS, YZ, and HH conceived the article. XY performed the experiments and conducted the analysis. YZ assisted with the analysis. ZW, RJ, JY, and ZC conducted ship-based sampling. XY, DS, YZ, and HH wrote the article.

Data Availability Statement: The dataset for N_2 fixation in the (sub)tropical western North Pacific, including values of particulate nitrogen (PN), limits of detection, the ^{15}N atom % of PN, volumetric N_2 fixation rates, and environmental parameters, has been published in a data repository (https://doi.org/10.6084/m9.figshare.24225457.v4) (Yu et al. 2023).

Additional Supporting Information may be found in the online version of this article.

Bioavailable nitrogen is a crucial factor limiting primary production in the global ocean (Zehr 2011; Moore et al. 2013). Nitrogen (N_2) fixation can provide new bioavailable nitrogen for supporting production and carbon sequestration (Karl and Letelier 2008; Sohm et al. 2011; Bonnet et al. 2016). The North Pacific Subtropical Gyre (NPSG) is one of the major sinks of carbon dioxide in the global ocean (Takahashi et al. 2009), despite the low nitrate concentrations in surface water (Moore et al. 2013). This suggests the potentially important role of N_2 fixation in fueling primary production in the region (Shiozaki et al. 2009; Böttjer et al. 2017). Recently, high N_2 fixation rates (> 10 nmol N L^{-1} d^{-1} volumetric rate and > 500 μmol N m^{-2} d^{-1} depth-integrated rate) were observed in the (sub)tropical western North Pacific (Wen et al. 2022*a*), covering approximately one-third of the NPSG area.

Previous observations have shown spatial variability in N_2 fixation rates in the western North Pacific. Specifically, rates can reach up to 10 nmol N L^{-1} d^{-1} between 20° N and 25° N, while they are typically near 0 nmol N L^{-1} d^{-1} in the northern and southern areas (Kitajima et al. 2009; Shiozaki et al. 2009; Wen et al. 2022*a*). The iron-to-nitrogen supply ratio is critical in regulating the distribution of N_2 fixation, and phosphate availability sets an upper bound on N_2 fixation rates (Wen et al. 2022*a*). Potential seasonal variations in N_2 fixation rates have also been observed in the western North Pacific along the Kuroshio Current (Chen et al. 2008). Nonetheless, owing to a limited number of observations, the spatiotemporal patterns and environmental controls of N_2 fixation rates in the western North Pacific remain poorly understood, restricting the assessment of regional N_2 fixation flux. High-resolution observations are thus urgently needed to fill this gap.

Although complete spatiotemporal coverage of in situ observations is currently unavailable, empirical models provide an effective way to predict N_2 fixation rates in under-sampled areas. However, despite the development of various models for estimating global marine N_2 fixation rates, significant uncertainties remain at the regional level. Taking the (sub)tropical western North Pacific as an example, some models suggest higher rates in this region than in other oceans (Paulsen et al. 2017; Wang et al. 2019), while others indicate the opposite (Landolfi et al. 2015; Jickells et al. 2017; Tang et al. 2019). These discrepancies are caused by different modeling mechanisms, such as different considerations of the utilization of organic phosphorus, the nitrogen budget balance, and grazing, etc. (Séférian et al. 2013; Landolfi et al. 2015; Wang et al. 2019). Selection of environmental factors and inconsistent values of parameters (e.g., the half-saturation constant of nutrients) also result in diverse estimates (Paulsen et al. 2017; Riche and Christian 2018). Additionally, insufficient observations in this region and the omission of seasonal variation by some models could attenuate the precision of estimations (Luo et al. 2014; Tang et al. 2019) (Supporting Information Fig. S1).

To improve the accuracy of regional N_2 fixation assessment, we conducted dense measurements of N_2 fixation rates in the (sub)tropical western North Pacific during various seasons from 2016 to 2021. Our new measurements, along with published observations, were used to estimate N_2 fixation flux and identify spatiotemporal patterns and environmental regulatory mechanisms in the western North Pacific via random forest (RF) and support vector regression (SVR).

Methods

Data for N_2 fixation rates included 273 new measurements and 64 published observations (Lu et al. 2019; Wen et al. 2022*a*,*b*; Shao et al. 2023). The new data were sampled in the northern South China Sea (NSCS) (111° E–120° E, 14° N–22° N) and the open ocean region (120° E–158° E, 11° N–33° N). The observations in the open ocean region were distributed in the western NPSG, the North Pacific Transition Zone (NPTZ), the North Equatorial Current (NEC), and the upstream Kuroshio (Fig. 1). Sampling details are given in the Supporting Information Data S1.

N_2 fixation rates were determined using the $^{15}N_2$ gas dissolution method (Mohr et al. 2010) and calculated as described by Montoya et al. (1996). Limits of detection (LOD) of samples were calculated following the best practice described by White et al. (2020). More details of measurement and calculation were described in Supporting Information Data S1. The N_2 fixation rates, the PN, the ^{15}N atom % of PN, and the LOD were summarized in a dataset (https://doi.org/10.6084/m9.figshare.24225457.v4, Yu et al. 2023).

N_2 fixation in the western North Pacific predominantly occur at depths shallower than 100 m (Lu et al. 2019; Wen et al. 2022*a*). Therefore, for the depth profile observations in Fig. 1c–h, 100 m depth-integrated N_2 fixation rates (INFRs) were calculated using the trapezoidal integration method. For the surface N_2 fixation observations in Fig. 1i–k, simple linear regression between surface N_2 fixation rates (SNFRs) and INFRs was derived and used to extrapolate SNFRs to INFRs (Supporting Information Fig. S2), as their correlation was significant ($r = 0.94$, $r^2 = 0.88$). After log-transforming INFRs, the RF and SVR models were used to predict the distributions of monthly INFRs from 2016 to 2020. Environmental parameters and model constructions are provided in the Supporting Information Data S1. Detailed information on comparing N_2 fixation fluxes across different oceans and calculating the contribution of N_2 fixation to primary productivity in the western North Pacific are described in Materials and Methods in the Supporting Information Data S1.

Results and discussion

Spatiotemporal patterns of observed N_2 fixation rates

Our observations revealed substantial spatiotemporal variability in N_2 fixation rates in the (sub)tropical western North Pacific, which ranged from below the LOD to nearly 31 nmol N L^{-1} d^{-1} for all samples. Among the measured rates, 89% were below 5 nmol N L^{-1} d^{-1} or even the LOD ($n = 457$) and 3% were over 10 nmol N L^{-1} d^{-1} ($n = 13$). In the open ocean region

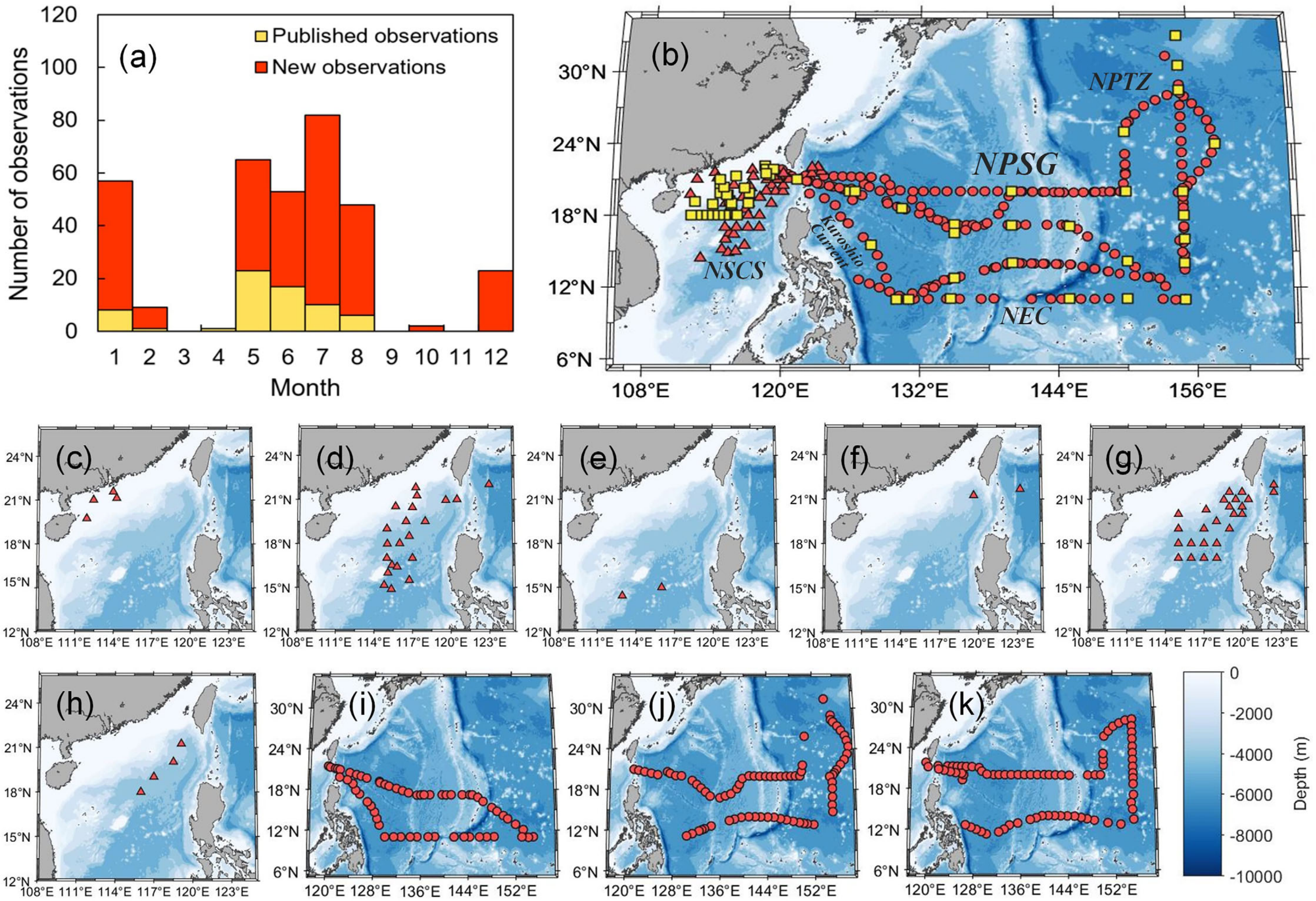

Fig. 1. (**a**) The seasonal distribution of the number of observations and (**b–k**) the spatial pattern of the sampling sites. Red triangles represent new observations of the depth profile of N_2 fixation rates within the upper 100 m, including (c) 4 observations during 05/2016–06/2016, (d) 21 observations during 07/2017–08/2017, (e) 2 observations in 05/2017, (f) 2 observations in 10/2017, (g) 25 observations during 06/2018–07/2018, and (h) 4 observations in 08/2018. Red circles represent new surface observations at a depth of 5 m, including (i) 60 observations during 05/2019–06/2019, (j) 76 observations during 07/2020–08/2020, and (k) 79 observations during 12/2020–02/2021. Yellow squares represent published depth profile observations that were acquired primarily in summer. The new observations span four seasons in the (sub)tropical western North Pacific.

(including the western NPSG, the NPTZ, the NEC, and the upstream Kuroshio), both SNFRs and INFRs exhibited greater intensities during spring–summer than in winter (Fig. 2). Specifically, average SNFRs and INFRs were 3.77 ± 3.95 (mean $\pm$ standard deviation) nmol N L^{-1} d^{-1} ($n = 145$) and 252.44 ± 221.40 μmol N m^{-2} d^{-1} ($n = 145$), respectively, during spring–summer, and decreased to 1.38 ± 1.62 nmol N L^{-1} d^{-1} ($n = 78$) and 75.12 ± 78.73 μmol N m^{-2} d^{-1} ($n = 78$) in winter. These values are numerically similar to previous observations in the North Pacific (Shiozaki et al. 2009; Chen et al. 2019). The large standard deviations reflect the inhomogeneous distribution of SNFRs and INFRs in space. Seasonal variation aligns with previously observed patterns of rates in the Kuroshio and the western NPSG (Chen et al. 2008, 2014) and with basin-scale observations of diazotroph abundance in the North Pacific (Cheung et al. 2020). In the NSCS, average INFRs were 156.14 ± 184.07 μmol N m^{-2} d^{-1} ($n = 47$) and 89.90 ± 100.31 μmol N m^{-2} d^{-1} ($n = 3$), respectively, during spring–summer and fall–winter. Despite the uneven temporal coverage, our observations spanned four seasons (Fig. 1), enabling us to track seasonal variability in the western North Pacific, which was previously poorly understood owing to a lack of in situ measurements.

During spring–summer, the spatial distribution of N_2 fixation rates in the western North Pacific was inhomogeneous (Fig. 2a,c). The Kuroshio Current exhibited the highest average SNFR (6.20 ± 5.69 nmol N L^{-1} d^{-1}, $n = 30$), followed by the western NPSG (4.03 ± 3.08 nmol N L^{-1} d^{-1}, $n = 86$) and the NSCS (2.54 ± 3.36 nmol N L^{-1} d^{-1}, $n = 46$). The lowest SNFR was observed in the NEC (0.44 ± 0.47 nmol N L^{-1} d^{-1}, $n = 28$).

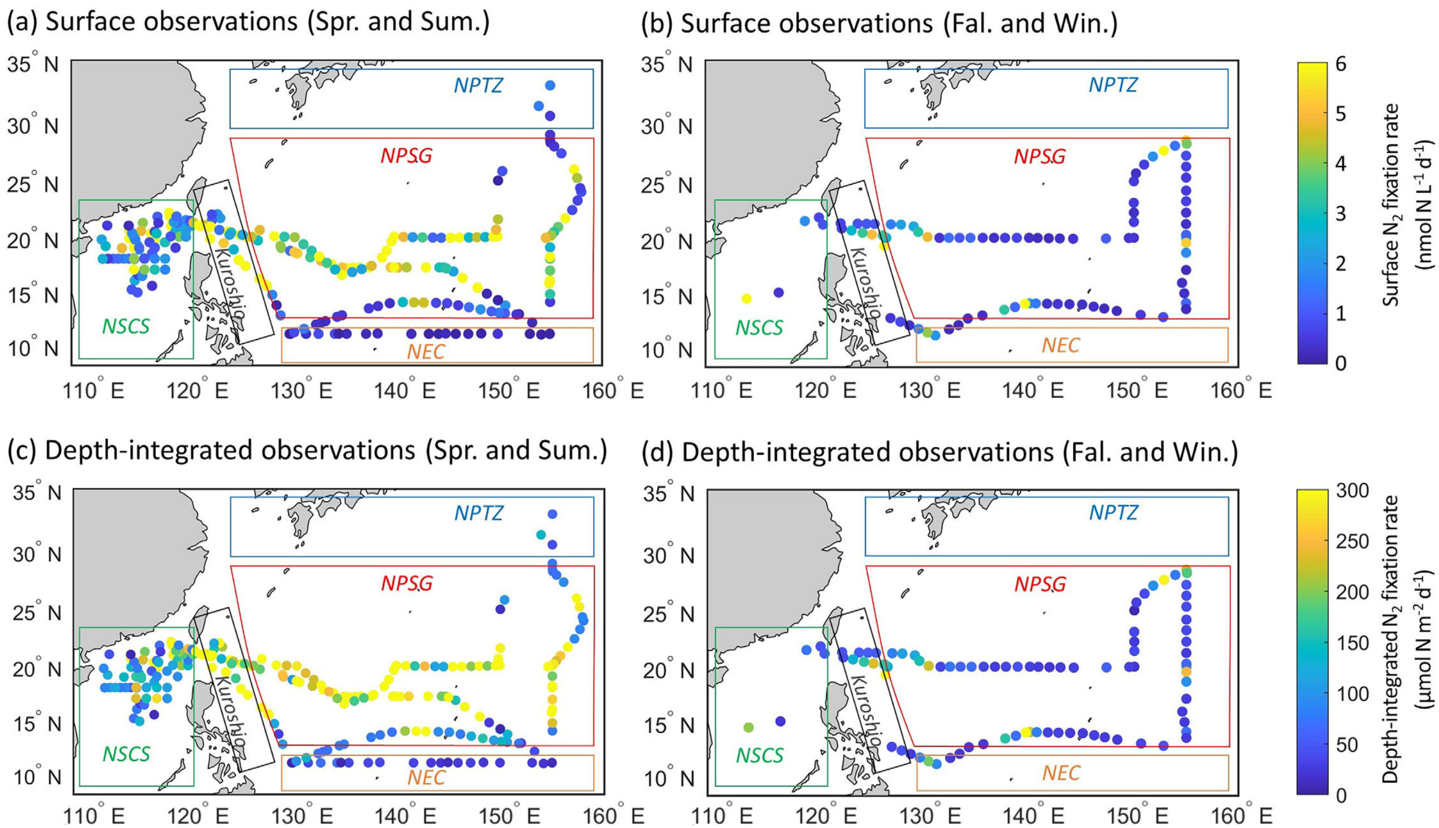

Fig. 2. Spatiotemporal patterns of observed N_2 fixation rates. The SNFRs are displayed in (**a**, **b**), and the INFRs are displayed in (**c**, **d**). The SNFRs and INFRs in (**a**, **c**) spring–summer (April to August) and in (**b**, **d**) fall–winter (October and December to February) are shown. The INFRs in the NSCS are calculated using the trapezoidal integration method based on the measurements of N_2 fixation rates at different depths. The INFRs in the open ocean region are extrapolated from SNFRs based on the linear relationships between SNFRs and INFRs as reported in this region (Supporting Information Fig. S2).

The spatial distribution of INFRs exhibited a similar pattern. Over 60% of the lower-end INFRs (< 30 μmol N m^{-2} d^{-1}, $n = 14$) were from the NEC ($n = 9$), with others distributed in the NSCS ($n = 4$) and the western NPSG ($n = 1$). The regions affected by the Kuroshio Current reported the highest average INFR (393.62 ± 310.92 μmol N m^{-2} d^{-1}, $n = 30$). The average INFR in the NPSG (268.59 ± 171.64 μmol N m^{-2} d^{-1}, $n = 86$) was 70% greater than that in the NSCS (156.14 ± 184.07 μmol N m^{-2} d^{-1}, $n = 47$). The observed spatial distribution was consistent with previous findings (Chen et al. 2008; Kitajima et al. 2009; Wen et al. 2022*a*). Additionally, a depth profile showed higher rates in the eastern NSCS compared to the western NSCS (Supporting Information Fig. S4), likely reflecting the influence of inflow from the Kuroshio Current (Lu et al. 2019). Our high-resolution observations provide a comprehensive understanding of the spatial gradient across the western North Pacific, underlining high N_2 fixation rates in this region.

Estimations of N_2 fixation rates

By using high-resolution observations and published data, we obtained accurate RF and SVR models to simulate INFRs, which enabled us to evaluate spatiotemporal patterns in the entire region. In the randomly divided testing dataset (20% of the total data), the estimated and observed INFRs generally converged onto the 1 : 1 line (Supporting Information Fig. S5a,b). The correlation coefficients reached 0.83 (RF) and 0.82 (SVR), indicating strong positive correlations between the estimations and observations. Although the slopes of the fitting curves were lower than 1, we achieved models with higher correlation coefficients and lower root mean square error (RMSE) compared with previous data-driven models that were limited by sparse observations (Luo et al. 2014; Tang et al. 2019) (Supporting Information Fig. S5c). The mean absolute errors were 1.54 (RF) and 1.50 (SVR) μmol N m^{-2} d^{-1}, demonstrating the overall accuracy of the models in predicting INFRs. Furthermore, both models accurately captured the seasonal and spatial variations in INFRs as observed in the testing dataset (Supporting Information Fig. S5d). Our models demonstrated that high-resolution observations, especially in winter, enhanced the reliability of estimating spatiotemporal variations of INFRs.

Using these models, we predicted continuous spatiotemporal patterns of INFRs throughout the entire region. The estimated regional N_2 fixation fluxes were 5.72 Tg N yr^{-1} (SVR) and 6.45 Tg N yr^{-1} (RF). The estimates consistently showed higher rates and fluxes during warm seasons compared with cold seasons (Fig. 3a–e). This seasonal variation was missing in previous estimations (Supporting Information Fig. S6a), emphasizing the importance of high-resolution observations across different seasons. No significant interannual variation was found, indicating that repeated observations over longer time scales are needed. Although the SVR estimates were lower than the RF estimates, both models concurred that the Kuroshio Current and the western NPSG were major contributors to regional N_2 fixation flux (Fig. 3f,g). This result contradicts previous models that indicated homogeny across the region and attributed greater flux to the NSCS than to the western NPSG and the Kuroshio Current (Luo et al. 2014; Tang et al. 2019) (Supporting Information Fig. S6b–d). Furthermore, our estimates of annual N_2 fixation flux in the entire region almost doubled the previous estimates (Supporting Information Table S2).

The (sub)tropical western North Pacific presented N_2 fixation fluxes that were notably greater than those in globally recognized ocean hotspots. Specifically, the tropical North Atlantic, the eastern NPSG, and the western tropical South Pacific reported average N_2 fixation fluxes per unit area of 3.36×10^{-7}, 4.47×10^{-7}, and 2.91×10^{-7} $\mathrm{Tg\,N\,km^{-2}\,yr^{-1}}$, respectively, per the SVR and RF models (Tang et al. 2019). In comparison, the western North Pacific had greater fluxes of 5.72×10^{-7} (SVR) and 6.45×10^{-7} (RF) $\mathrm{Tg\,N\,km^{-2}\,yr^{-1}}$ (Supporting Information Table S3). This difference emphasizes the global importance of N_2 fixation in the western North Pacific. Additionally, in the western NPSG, N_2 fixation was estimated to contribute up to 9.2% (RF) or 6.7% (SVR) to net primary production (Supporting Information Fig. S7). These findings highlight the critical role of N_2 fixation in supporting productivity in oligotrophic (sub)tropical oceans (Raimbault and Garcia 2008; Shiozaki et al. 2013; Benavides et al. 2013*a*).

Environmental controls of N_2 fixation rates

Our study identified the best predictors for estimating INFRs with minimum RMSE using the RF algorithm, including Coordinate1, Month1, PAR, iron deposition flux (Fe_{dep}), Coordinate3, surface dissolved oxygen (DO), and sea surface temperature (SST) (Fig. 4a). The Month1 component comprised sampling months converted by Supporting Information eq. S3, and the Coordinate1 and Coordinate3 components comprised sampling latitudes and longitudes converted by Eq. S4. These predictors were selected from 30 environmental parameters (Supporting Information Table S1) and explained 68% of the variability in actual INFRs in both RF and SVR models (Supporting Information Fig. S5a,b), suggesting that they controlled the spatiotemporal variation in INFRs.

In the western North Pacific, SST and PAR are expected to be related to seasonal variation in INFRs (Figs. 2 and 4b–e). A higher SST and PAR (29.6 °C and 829.6 $\mu\mathrm{mol\,m^{-2}\,s^{-1}}$, regional average) during spring–summer than during fall–winter (26.6 °C and 596.5 $\mu\mathrm{mol\,m^{-2}\,s^{-1}}$, regional average) can enhance the activity of nitrogenase and provide favorable conditions for cellular metabolic energy production in diazotrophs, which are essential for N_2 fixation (Staal et al. 2003; Fu et al. 2014; Lu et al. 2018). Month1 served as a composite indicator reflecting seasonal variation in SST and PAR (Fig. 4f,g).

The mechanism by which DO in seawater affects N_2 fixation has not been determined (Tang et al. 2019). We hypothesize that DO serves as a combined predictor that primarily represents SST, as these two predictors exhibit a strong correlation ($r = -0.70$, $p < 0.001$) (Supporting Information Fig. S8a). Additionally, DO was also related to the supply ratio of iron to nitrogen ($Fe_{total} : N_{total}$) ($r = 0.36$, $p < 0.001$), sea surface salinity (SSS) ($r = 0.33$, $p < 0.001$), Fe_{dep} ($r = 0.30$, $p < 0.001$), and the subsurface supply rate of phosphate (P_{up}) ($r = -0.23$, $p < 0.001$). Although some of these regulators were not identified individually by the RF algorithm, they may also be important to N_2 fixation. For instance, the gradient of $Fe_{total} : N_{total}$ was found to be consistent with that of diazotroph abundances and N_2 fixation rates in the upper ocean of this region (Wen et al. 2022*a*). P_{up} was positively correlated with the subsurface supply rate of nitrogen (N_{up}) ($r = 0.87$, $p < 0.001$), thereby exhibiting a negative correlation with INFRs (Supporting Information Table S1). The spatial pattern of SSS distinguished different intensities of INFRs in the NSCS and the open ocean region (Supporting Information Fig. S8d).

High Fe_{dep} could stimulate the growth of diazotrophs and also promote N_2 fixation rates (Moore et al. 2009; Sohm et al. 2011; Benavides et al. 2013*b*). Fe_{dep}, the main source of dissolved iron in the western North Pacific (Supporting Information Fig. S8e–h) (Brown et al. 2005; Hsu et al. 2009; Wen et al. 2022*a*), is a crucial nutrient for nitrogenase to function (Schindelin et al. 1997). Although Fe_{dep} was higher during fall–winter than during spring–summer (Supporting Information Fig. S8e,f), there may be a time lag in the conversion of iron from atmospheric deposition to bioavailability and absorption by diazotrophs (Tan and Wang 2014; Tang et al. 2021). Furthermore, the spatial distributions of Fe_{dep} and the observed INFRs were not always consistent (Fig. 4h,i), indicating that although Fe_{dep} is hypothesized to play an important role, it was not the only factor controlling the spatial pattern of INFRs.

Coordinate1 was a location predictor and was correlated with depth-integrated phosphate (IDIP) ($r = -0.40$, $p < 0.001$), mixed layer depth (MLD) ($r = -0.37$, $p < 0.001$), SST ($r = -0.36$, $p < 0.001$), SSS ($r = 0.34$, $p < 0.001$), and N_{up} ($r = -0.34$, $p < 0.001$) (Supporting Information Fig. S8b). The negative correlation between INFRs and IDIP indicates that phosphate reflects the residual effect of nutrient consumption caused by N_2 fixation rather than the facilitating effect of nutrient supply (Supporting Information Table S1) (Shiozaki et al. 2018).

Coordinate3 primarily reflected nitrate-related information and was strongly correlated with the depth of chlorophyll maximum (DCM) ($r = 0.71$, $p < 0.001$) and the nitracline ($r = 0.70$, $p < 0.001$) (Supporting Information Fig. S8c). A

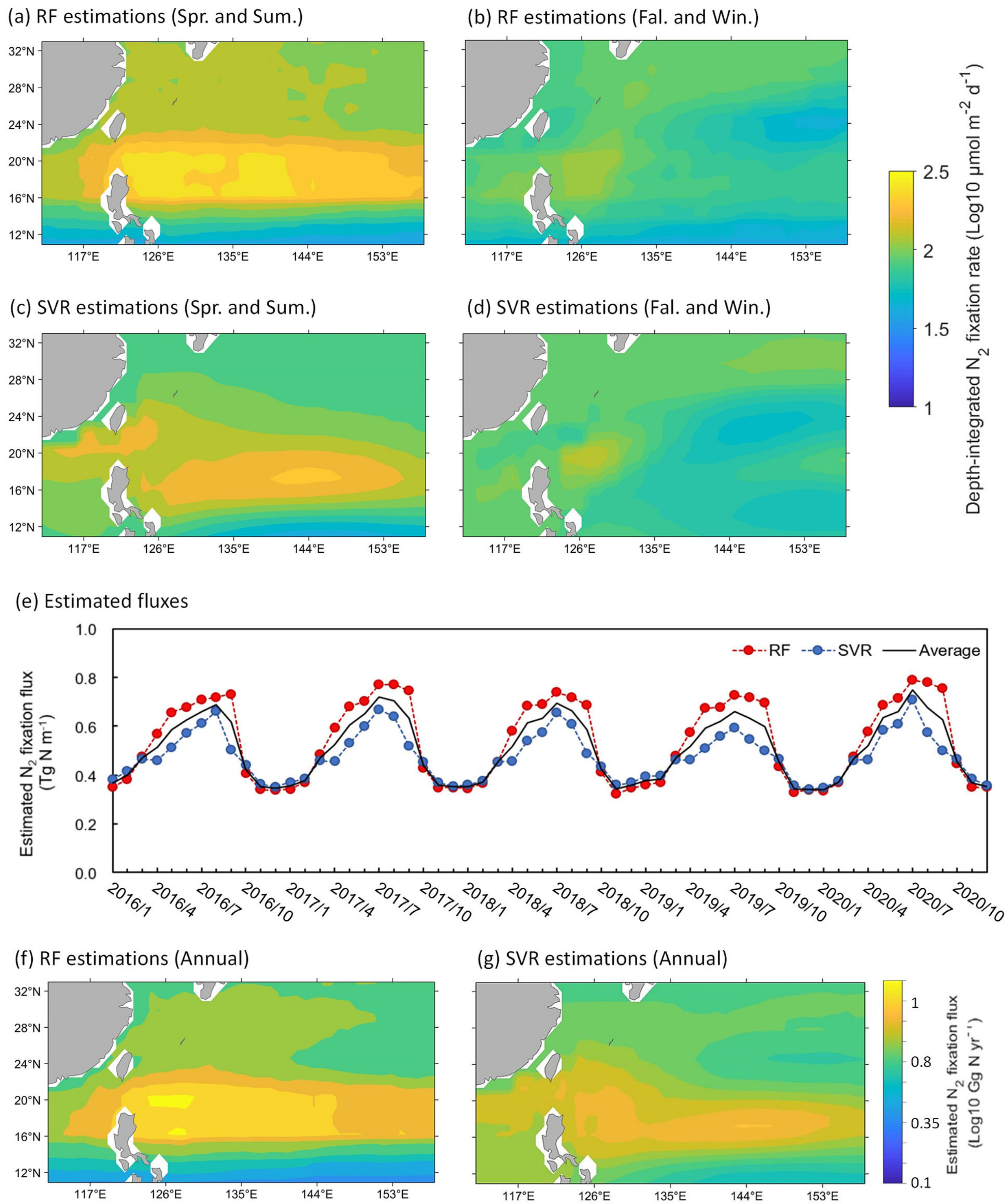

Fig. 3. The estimated N_2 fixation rates and fluxes. (**a**, **b**) The RF model and (**c**, **d**) the SVR model effectively reproduced INFRs in the entire region. INFRs shown in (a, c) represent average estimates from April to August, while those shown in (b, d) represent average estimates from October and December to February. (**e**) The regional monthly fluxes from 2016 to 2020 estimated by the two models showed consistent seasonal variation. (**f**, **g**) The spatial distributions of fluxes were calculated by summing the estimated monthly fluxes.

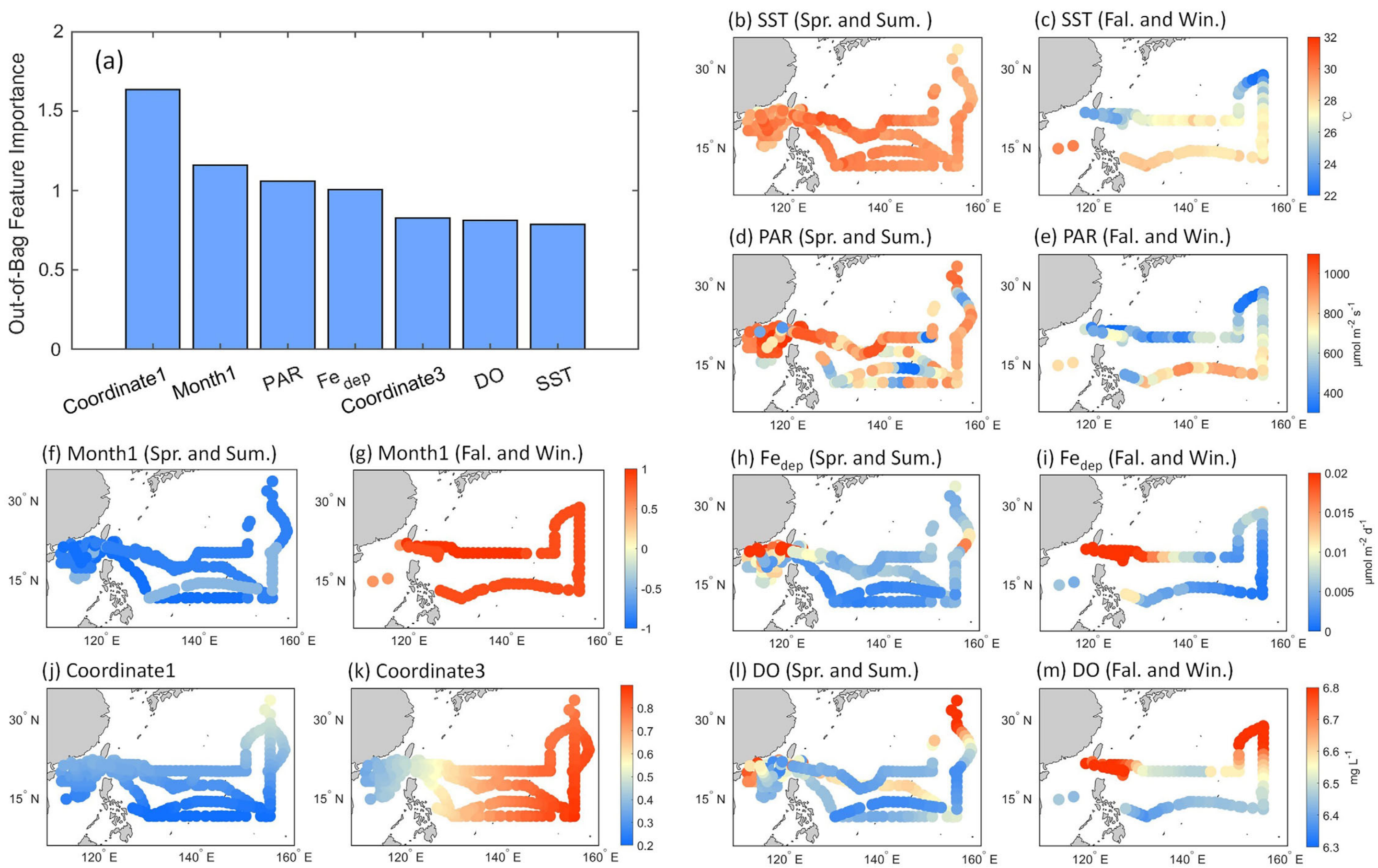

Fig. 4. The best predictors and their spatial distribution in different seasons (all points matched the sampling months and locations). (**a**) The best predictors were calculated by the RF algorithm and included (**b**, **c**) SST, (**d**, **e**) PAR, (**f**, **g**) Month 1, (**h**, **i**) Fe_{dep}, (**j**) Coordinate1, (**k**) Coordinate3, and (**l**, **m**) DO.

deeper nitracline could limit the subsurface supply of nitrate to the sea surface, potentially hindering nondiazotrophic phytoplankton growth but providing an advantage for diazotrophs. Combined with Fe_{dep}, it has been suggested that regions with high iron and low nitrate are particularly suitable for N_2 fixation (Ward et al. 2013; Wen et al. 2022*a*). The spatial distribution of the DCM was consistent with that of the nitracline, characterized by shallower values in the NSCS and deeper values in the open ocean region. Coordinate3 was also correlated with the ratio of depth-integrated nitrogen to phosphorus (IDIN : IDIP) ($r = -0.69$, $p < 0.001$), MLD ($r = 0.69$, $p < 0.001$), and depth-integrated dissolved iron (IdFe) ($r = -0.64$, $p < 0.001$). The combined predictors, such as Coordinate1, Coordinate3, and Month1, may reflect the complex coupling relationships between different environmental factors, which should have important impacts on N_2 fixation in real oceanic conditions.

Conclusions

This study expanded our existing knowledge of N_2 fixation rates in the (sub)tropical western North Pacific by providing high-resolution observations. N_2 fixation rates showed significant spatiotemporal patterns, with the highest rates occurring in summer. The N_2 fixation fluxes across the entire region were estimated to reach 5.72 (SVR) and 6.45 (RF) Tg N yr^{-1}, higher than other globally recognized ocean N_2 fixation hotspots. The western NPSG and the Kuroshio Current contributed more to N_2 fixation fluxes than did adjacent areas. Sea surface temperature, photosynthetically available radiation, and nutrient supply (iron, phosphate, and nitrogen) were identified as the key environmental factors that related to the spatiotemporal variations estimated by the RF algorithm. These findings have important implications for studies of ocean biogeochemistry and global carbon cycles.

References

Benavides, M., D. A. Bronk, N. S. R. Agawin, P. H. M. Dolores, A. Hernández-Guerra, and J. Arístegui. 2013*a*. Longitudinal variability of size-fractionated N_2 fixation and DON release rates along 24.5° N in the subtropical North Atlantic. J. Geophys. Res. Oceans **118**: 3406–3415. doi:10.1002/jgrc.20253

Benavides, M., J. Arístegui, N. S. R. Agawin, J. L. Cancio, and S. Hernández-León. 2013*b*. Enhancement of nitrogen fixation rates by unicellular diazotrophs vs.Trichodesmium after a dust deposition event in the Canary Islands. Limnol. Oceanogr. **58**: 267–275. doi:10.4319/lo.2013.58.1.0267

Bonnet, S., H. Berthelot, K. Turk-Kubo, S. Fawcett, E. Rahav, S. L' Helguen, and I. Berman-Frank. 2016. Dynamics of N_2 fixation and fate of diazotroph-derived nitrogen in a low-nutrient, low-chlorophyll ecosystem: Results from the VAHINE mesocosm experiment (New Caledonia). Biogeosciences **13**: 2653–2673. doi:10.5194/bg-13-2653-2016

Böttjer, D., J. E. Dore, D. M. Karl, R. M. Letelier, C. Mahaffey, S. T. Wilson, J. Zehr, and M. J. Church. 2017. Temporal variability of nitrogen fixation and particulate nitrogen export at station ALOHA. Limnol. Oceanogr. **62**: 200–216. doi:10.1002/lno.10386

Brown, M. T., W. M. Landing, and C. I. Measures. 2005. Dissolved and particulate Fe in the western and central North Pacific: Results from the 2002 IOC cruise. Geochem. Geophys. Geosyst. **6**: Q10001. doi:10.1029/2004GC000893

Chen, M. M., Y. Y. Lu, N. Z. Jiao, J. W. Tian, S.-J. Kao, and Y. Zhang. 2019. Biogeographic drivers of diazotrophs in the western Pacific Ocean. Limnol. Oceanogr. **64**: 1403–1421. doi:10.1002/lno.11123

Chen, Y.-L.L., H. Y. Chen, S. H. Tuo, and K. Ohki. 2008. Seasonal dynamics of new production from Trichodesmium N_2 fixation and nitrate uptake in the upstream Kuroshio and South China Sea basin. Limnol. Oceanogr. **53**: 1705–1721. doi:10.4319/lo.2008.53.5.1705

Chen, Y.-L.L., H. Y. Chen, Y. H. Lin, T. C. Yong, Y. Taniuchi, and S. H. Tuo. 2014. The relative contributions of unicellular and filamentous diazotrophs to N_2 fixation in the South China Sea and the upstream Kuroshio. Deep Sea Res. Part I-Oceanogr. Res. Pap. **85**: 56–71. doi:10.1016/j.dsr.2013.11.006

Cheung, S. Y., and others. 2020. Physical forcing controls the basin-scale occurrence of nitrogen-fixing organisms in the North Pacific Ocean. Geophys. Res. Lett. **34**: e2019GB006452. doi:10.1029/2019GB006452

Fu, F. X., E. Yu, N. S. Garcia, J. Gale, Y. Luo, E. A. Webb, and D. A. Hutchins. 2014. Differing responses of marine N_2 fixers to warming and consequences for future diazotroph community structure. Aquat. Microb. Ecol. **72**: 33–46. doi:10.3354/ame01683

Hsu, S.-C., S. C. Liu, R. Arimoto, T.-H. Liu, Y.-T. Huang, F. Tsai, F.-J. Lin, and S.-J. Kao. 2009. Dust deposition to the East China Sea and its biogeochemical implications. J. Geophys. Res. Atmos. **114**: D15304. doi:10.1029/2008JD011223

Jickells, T. D., and others. 2017. A reevaluation of the magnitude and impacts of anthropogenic atmospheric nitrogen inputs on the ocean. Glob. Biogeochem. Cycle **31**: 289–305. doi:10.1002/2016GB005586

Karl, D. M., and R. M. Letelier. 2008. Nitrogen fixation-enhanced carbon sequestration in low nitrate, low chlorophyll seascapes. Mar. Ecol. Prog. Ser. **364**: 257–268. doi:10.3354/meps07547

Kitajima, S., K. Furuya, F. Hashihama, S. Takeda, and J. Kanda. 2009. Latitudinal distribution of diazotrophs and their nitrogen fixation in the tropical and subtropical western North Pacific. Limnol. Oceanogr. **54**: 537–547. doi:10.4319/lo.2009.54.2.0537

Landolfi, A., W. Koeve, H. Dietze, P. Kähler, and A. Oschlies. 2015. A new perspective on environmental controls of marine nitrogen fixation. Geophys. Res. Lett. **42**: 4482–4489. doi:10.1002/2015GL063756

Lu, Y. Y., Z. Z. Wen, D. L. Shi, M. M. Chen, Y. Zhang, S. Bonnet, Y. H. Li, J. W. Tian, and S.-J. Kao. 2018. Effect of light on N_2 fixation and net nitrogen release of Trichodesmium in a field study. Biogeosciences **15**: 1–12. doi:10.5194/bg-15-1-2018

Lu, Y. Y., Z. Z. Wen, D. L. Shi, W. F. Lin, S. Bonnet, M. H. Dai, and S.-J. Kao. 2019. Biogeography of N_2 fixation influenced by the western boundary current intrusion in the South China Sea. J. Geophys. Res. Oceans **124**: 6983–6996. doi:10.1029/2018JC014781

Luo, Y. W., I. D. Lima, D. M. Karl, C. A. Deutsch, and S. C. Doney. 2014. Data-based assessment of environmental controls on global marine nitrogen fixation. Biogeosciences **11**: 691–708. doi:10.5194/bg-11-691-2014

Mohr, W., T. Grosskopf, D. W. Wallace, and J. LaRoche. 2010. Methodological underestimation of oceanic nitrogen fixation rates. PLoS One **5**: e12583. doi:10.1371/journal.pone.0012583

Montoya, J. P., M. Voss, P. Kähler, and D. G. Capone. 1996. A simple, high-precision, high-sensitivity tracer assay for N_2 fixation. Appl. Environ. Microbiol. **62**: 986–993. doi:10.1128/aem.62.3.986-993.1996

Moore, C. M., and others. 2009. Large-scale distribution of Atlantic nitrogen fixation controlled by iron availability. Nat. Geosci. **2**: 867–871. doi:10.1038/ngeo667

Moore, C. M., and others. 2013. Processes and patterns of oceanic nutrient limitation. Nat. Geosci. **6**: 701–710. doi:10.1038/ngeo1765

Paulsen, H., T. Ilyina, K. D. Six, and I. Stemmler. 2017. Incorporating a prognostic representation of marine nitrogen fixers into the global ocean biogeochemical model HAMOCC. J. Adv. Model. Earth Syst. **9**: 438–464. doi:10.1002/2016MS000737

Raimbault, P., and N. Garcia. 2008. Evidence for efficient regenerated production and dinitrogen fixation in nitrogen-deficient waters of the South Pacific Ocean: Impact on new and export production estimates. Biogeosciences **5**: 323–338. doi:10.5194/bg-5-323-2008

Riche, O. G. J., and J. R. Christian. 2018. Ocean dinitrogen fixation and its potential effects on ocean primary production in earth system model simulations of anthropogenic warming. Elem. Sci. Anthrop. **6**: 16. doi:10.1525/elementa.277

Schindelin, H., C. Kisker, J. L. Schlessman, J. B. Howard, and D. C. Rees. 1997. Structure of ADP x AIF4(−)-stabilized nitrogenase complex and its implications for signal transduction. Nature **387**: 370–376. doi:10.1038/387370a0

Séférian, R., and others. 2013. Skill assessment of three earth system models with common marine biogeochemistry. Climate Dynam. **40**: 2549–2573. doi:10.1007/s00382-012-1362-8

Shao, Z. B., and others. 2023. Global oceanic diazotroph database version 2 and elevated estimate of global oceanic N_2 fixation. Earth Syst. Sci. Data **15**: 3673–3709. doi:10.5194/essd-15-3673-2023

Shiozaki, T., K. Furuya, T. Kodama, and S. Takeda. 2009. Contribution of N_2 fixation to new production in the western North Pacific Ocean along 155° E. Mar. Ecol. Prog. Ser. **377**: 19–32. doi:10.3354/meps07837

Shiozaki, T., T. Kodama, S. Kitajima, M. Sato, and K. Furuya. 2013. Advective transport of diazotrophs and importance of their nitrogen fixation on new and primary production in the western Pacific warm pool. Limnol. Oceanogr. **58**: 49–60. doi:10.4319/lo.2013.58.1.0049

Shiozaki, T., and others. 2018. Linkage between dinitrogen fixation and primary production in the oligotrophic South Pacific Ocean. Glob. Biogeochem. Cycle **32**: 1028–1044. doi:10.1029/2017GB005869

Sohm, J. A., E. A. Webb, and D. G. Capone. 2011. Emerging patterns of marine nitrogen fixation. Nat. Rev. Microbiol. **9**: 499–508. doi:10.1038/nrmicro2594

Staal, M., F. J. R. Meysman, and L. J. Stal. 2003. Temperature excludes N_2-fixing heterocystous cyanobacteria in the tropical oceans. Nature **425**: 504–507. doi:10.1038/nature01999

Takahashi, T., and others. 2009. Climatological mean and decadal change in surface ocean pCO_2, and net sea-air CO_2 flux over the global oceans. Deep Sea Res. Part II Top. Stud. Oceanogr. **56**: 554–577. doi:10.1016/j.dsr2.2008.12.009

Tan, S.-C., and H. Wang. 2014. The transport and deposition of dust and its impact on phytoplankton growth in the Yellow Sea. Atmos. Environ. **99**: 491–499. doi:10.1016/j.atmosenv.2014.10.016

Tang, W. Y., Z. C. Li, and N. Cassar. 2019. Machine learning estimates of global marine nitrogen fixation. J. Geophys. Res. Biogeosci. **124**: 717–730. doi:10.1029/2018JG004828

Tang, W. Y., and others. 2021. Widespread phytoplankton blooms triggered by 2019-2020 Australian wildfires. Nature **597**: 370–375. doi:10.1038/s41586-021-03805-8

Wang, W. L., J. K. Moore, A. C. Martiny, and F. W. Primeau. 2019. Convergent estimates of marine nitrogen fixation. Nature **566**: 205–211. doi:10.1038/s41586-019-0911-2

Ward, B. A., S. Dutkiewicz, C. M. Moore, and M. J. Follows. 2013. Iron, phosphorus, and nitrogen supply ratios define the biogeography of nitrogen fixation. Limnol. Oceanogr. **58**: 2059–2075. doi:10.4319/lo.2013.58.6.2059

Wen, Z. Z., and others. 2022*a*. Nutrient regulation of biological nitrogen fixation across the tropical western North Pacific. Sci. Adv. **8**: eabl7564. doi:10.1126/sciadv.abl7564

Wen, Z. Z., and others. 2022*b*. The response of diazotrophs to nutrient amendment in the South China Sea and western North Pacific. Biogeosciences **19**: 5237–5250. doi:10.5194/bg-19-5237-2022

White, A. E., and others. 2020. A critical review of the $^{15}N_2$ tracer method to measure diazotrophic production in pelagic ecosystems. Limnol. Oceanogr. Meth. **18**: 129–147. doi:10.1002/lom3.10353

Yu, X. R., Z. Z. Wen, R. T. Jiang, J. Y. Yang, Z. M. Cao, H. Z. Hong, Y. T. Zhou, and D. L. Shi. 2023. *N_2 fixation in the (sub)tropical western North Pacific.Xlsx*. Figshare. Dataset. doi:10.6084/m9.figshare.24225457

Zehr, J. P. 2011. Nitrogen fixation by marine cyanobacteria. Trends Microbiol. **19**: 162–173. doi:10.1016/j.tim.2010.12.004

Acknowledgments

This study was supported by the National Natural Science Foundation of China (No. 41925026, No. 41890802), the National Key Research and Development Program of China (2023YFF0805004), and the National Natural Science Foundation of China (No. 92258302, No. 42341201, and No. 42276201). We thank all scientists, captains, and crews of the R/V *Tan Kah Kee* and the R/V *Dongfanghong 2* for assistance with the experiments in the field. We thank Ze Chen for help with LOD calculations and thank Lifang Wang, Tao Huang, Yanping Xu, and Chuanjun Du for help with nutrients and nitracline analysis. We also thank Weiyi Tang and Yawei Luo for providing their model results. We acknowledge the Community Earth System Model project and the Coupled Model Intercomparison Project for providing access to the model outputs. We would like to thank National Centers for Environmental Prediction reanalysis, World Ocean Atlas, Copernicus Marine Environment Monitoring Service, and Chia-Te Chien for making some parameters publicly available.

Submitted 25 December 2023
Revised 11 April 2024
Accepted 20 April 2024